AN ALGEBRAIC TURBULENCE MODEL WITH MEMORY FOR THE COMPUTATION OF THREE DIMENSIONAL TURBULENT BOUNDARY LAYERS

T. D. Hsing
Fluid Mechanics Institute
Beijing University of Aeronautics and Astronautics
Beijing, 100083, P. R. China

Abstract

Additional equations were found based on experiments for an algebraic turbulence model to improve the prediction of the behavior of three dimensional turbulent boundary layers by taking account of the effects of pressure gradient and the historical variation of eddy viscosity, therefore the model is with memory. Numerical calculation by solving boundary layer equations was carried out for five pressure driven three dimensional turbulent boundary layers developed on flat plates. swept–wing and prolate spheroid in symmetrical plane. Comparing the computational results with the experimental data, it is obvious that the predition will be more accurate, if the proposed closure equations are used, especially for the turbulent shear stresses.

Nomenclature

x, y, z	Cartesian coordinate fixed on the flat plate
s, y, n	local streamwise coordinate, with the s–axis in sense of velocity outside the boundary layer
u, v, w	mean velocity components along the x, y, z axis
u_s, v_y, w_n	mean velocity components along the s, y, n axis
u_r	$=(u_s^2+w_n^2)^{1/2}$
q	$=\frac{1}{2}\rho u_r^2$, dynamic pressure
u'_r	fluctuation of velocity u_r
τ	local shear stress
τ_w	wall friction
u_τ	$=(\tau_w/\rho)^{1/2}$, frictional velocity
u_r^+	u_r/u_τ
y^+	$=yu_\tau/\gamma$
η	$\eta=y/d, d=\sqrt{\frac{\nu x}{ue}}$
δ, δ^*, θ	thickness, displacement thickness and momentum thickness of the boundary layer respectively
H	$=\delta^*/\theta$, boundary layer shape factor
k	$=(\overline{u'^2}+\overline{v'^2}+\overline{w'^2})/2$ turbulent kinetic energy per unit mass
ε	rate of dissipation of turbulent kinetic energy
p	static pressure
C_p	$=(p-p_\infty)/\frac{1}{2}\cdot\rho u_\infty^2$), static pressure coefficient
C_f	$=\tau_w/(\frac{1}{2}\cdot\rho u_\infty^2)$, skin friction coefficient
ρ	air density
l	mixing length of turbulence
α	angle of wedge deflection, or wing angle of attack
β	$=tan^{-1}(w_n/u_s)$, angle between local and external streamline direction measured parallel to the surface
	or $=(dp/dx)(\delta^*/\tau_w)$, pressure gradient parameter
μ, ν, γ_t	dynamic, kinematic and eddy viscosity respectively

Subscripts

e	outer edge of the boundary
w	wall
∞	free–stream
eq	in equilibrium state
t	turbulent

I. Introduction

In recent years, the prediction of the viscous flow developed over three dimensional bodies, such as wings and fuselages, becomes important in the field of aerodynamics. The continuing advances in computational method and the rapid increase of computing power are enabling the research to proceed in solving the full Navier–Stokes equations. However, it seems that in the near future, there will still be a great need to meet the increasing demand in the aeronautical industry by using schemes which couple an inviscid flow solver to a boundary layer calculation method for evaluating the aerodynamic characteristics of airplane components. The aerodynamic researches in the field of three dimensional boundary layer are generally concentrated on the turbulent flow because of the high

The research was sponsored by the National Natural Science Foundation of China under Grant 83L04.

Reynolds number met in the aeronautical problems. Basically there are two approaches to turbulence modelling the Reynolds–averaged equations. They are algebraic and differential models according to whether the closure equations are of algebraic or differential form. Generally the algbraic turbulence models are more commonly used within the design environment because of their simplicity and versatility without the excessive requirements of computer memory and CPU time to aggravate the difficulties encountered in complex computation in aerodymic design. The other reason may be having less experience in setting boundary conditions for using differential turbulence models, such as the k–ε two equation model in treating the wall law or the added terms on account of the low Reynolds number effects in the case of flow with strong pressure gradient or on approaching the separation point which is not known in advance.

Nevertheless there are inherent demerits of the algebraic turbulence models, such as they are appropriate only for dealing with the equilibrium boundary layers and havn't taken the historical influence of the momentum transfer effects into account. Some of these demerits have been compensated in the revised two dimensional turbulence modelling to give good results . However, as to the three dimensional turbulent boundary layers, the computational results are less satisfiable especially for the shear stresses, because physically there exist the velocity skewness and the anisotropic distribution of the eddy viscosity within the boundary layer, which haven't been reckoned in the three dimensional modelling as it was generally deduced from the two dimensional models. It is believed that some of the three dimensional features can be taken into account, if the distribution of mixing length l or eddy viscosity ν_t is to be modified within the frame of altering the gradient $K=\frac{\partial l}{\partial y}$ in the inner layer and the maximum ratio of mixing length $C=(\frac{l}{\delta})_{max}$ in the outer layer, because K and C are quantitative parameters able to reflect the variation of the turbulence structure which can be affected by extra rates of strain under the action of pressure gradient. Actually our former experiments[1] did demonstrate that the streamwise and transverse pressure gradients would clearly influence the parameters K and C. The computational work[2]also reveals that by using the conventional models[3] without considering the influence of pressure gradient, e.g. Michel's model, the computational turbulent stresses would deviate apparently from the experimental results, although the bulk magnitude, e.g. mean velocity or boundary layer thickness, would agree better to the experiment. Therefore, it seems possible that the predictional accuracy could be improved, if the effects of the streamwise and transverse pressure gradients as well as the historical variation of the eddy viscosity or mixing length were taken into account by introducing additional closure equations. The investigation described below will bring on promisingly the intended outcome.

Ⅱ. Experimental procedure and turbulence modelling

In order to investigate the main influence of the pressure gradients on the distribution of mixing length and to find out the closure equations for turbulence modelling, experimental procedure was arranged.

Experimental study of the influence of streamwise pressure gradient on mixing length distribution

For the purpose of finding the influence of streamwise pressure gradient $\frac{\partial C_p}{\partial s}$ on mixing length slope $\frac{\partial l}{\partial y}$ and maximum mixing length ratio $(\frac{l}{\delta})_{max}$, flow along a flat plate with a wedge laid on it was studied. (See Fig.1). The pressure gradient $\frac{\partial C_p}{\partial s}$ in front of the wedge increases rapidly as the wedge is approached, and can be changed by varying the wedge angle α. In this case, the transverse pressure gradient $\frac{\partial C_p}{\partial n}$ is zero because of the two dimensionality, and the velocity beyond the boundary layer varies nearly as $u=cx^a$, where c and a are constants, near the wedge front, although the flow may separate slightly as verified by experiment. Taking the case $\alpha=29°$ for example, the velocity distribution calculated by this expression and by solving the potential equation (panel method) are nearly the same. The pressure coefficient C_p corresponding to the latter result is well agree to the experiment. (See Fig.2). Therefore this boundary layer flow can be recognized as in a state of equilibrium[4][5], and the experimental results so obtained will be suitable for modifying the algebraic turbulence models which is appropriate only for equilibrium boundary layer.

The experiment was carried out in BUAA in a low speed wind tunnel having a test–section of 0.92 × 0.92m in area and 1.52m long. The free stream velocity was kept at 16 m / s with turbulence intensity below 0.5% and Reynolds number 1×10^6 1 / m. By varying the wedge angle α, the pressure gradient or parameter $\beta=(dp/dx)(\delta^*/\tau_w)$ can be changed . The skin friction was measured by using Preston tube and surface hot film technique. By setting hot–wire and hot–film anemometers horizontally or vertically, could the mean velocity components u,v, u_r, and the turbulence quantities $\overline{u'^2}, \overline{v'^2}, \overline{u'v'}$ be determined. The measuring stations located in front of the wedge are as shown in Fig.1. It was observed that for various plate deflections α, the velocity profiles in form of the defect law (i.e. $\frac{u_e-u}{u_\tau}$ *vs.*

$\frac{y}{\delta}$) can be recognized as nearly independent of the measuring positions.(See Fig.3). This fact also confirms the flow within the boundary layer can be treated as in equilibrium [3]. The experimental results including the boundary thickness δ, δ^*, the distribution of $\frac{u}{u_e}$ vs. $\frac{y}{\delta}$ and the correlation $\overline{u'v'}/u_e^2$ vs. y/δ were obtained. From these data the mixing length distribution along the normal direction y can be determined based on the definition: $l=(-\overline{u'v'})^{\frac{1}{2}}/\left|\frac{\partial u}{\partial y}\right|$. Hence the derivative $K=\partial l/\partial y$ and the maximum mixing length $C=l_{max}/\delta$ against y/δ at the measuring stations were obtained. Since δ, τ_w, and $\frac{\partial p}{\partial x}$ had been determined earlier, the value of β was known. Finally the relations between K and β as well as C and β were derived[23]. (See Fig.4). These relations show that when $\beta<1.2$, K increases with β like the result given in Ref.6, and K decreases with β when $\beta>1.2$, while C decreases monotonically from $C=0.09$ at $\beta=0$ with the increase of β. These relationships can be reduced into two additional empirical formulas appropriate for computational application as follows:

$$K_{eq}=\begin{cases}0.40+0.18[1-exp(-0.32\beta)], & 0\leqslant\beta\leqslant 1.2\\ 0.374+0.005(5.5-\beta)^{1.93}, & 1.2<\beta\leqslant 5\\ 0.375-0.0037(\beta-5.0), & \beta>5\end{cases} \quad (1)$$

$$C_{eq}=\begin{cases}0.09-0.0053\beta, & \beta\leqslant 4\\ 0.069-0.0012(\beta-4.0) & \beta>4\end{cases} \quad (2)$$

where the footnote eq denotes equilibrium.

In addition, from the power spectrum records (see Fig.5), it was found that the maximum turbulent kinetic energy appearing at lower frequency becomes greater as moving towards the wedge corner. This phenomena might be explained as there were large eddies existing in the boundary layer and becoming stronger to bring about the extra rates of strain affecting the turburence structure and the change of K and C.

Experimental study of the influence of transverse pressure gradient on mixing length distribution

It remains to study the effect of transverse pressure gradiant $\frac{\partial C_p}{\partial n}$ on the three dimensional turbulent boundary layer. For this purpose, we ought to establish a flow field with $\frac{\partial C_p}{\partial n}\neq 0$ while $\frac{\partial C_p}{\partial s}=0$. Concerning this problem we have experienced from the former experiments[11] that the three dimensional turbulent boundary layer suitable for carrying out this research should satisfy at least: (1) no apparent vortical movement induced by the secondary flow under the action of centrifugal force , (2) no severe shearing action existing within the measuring area. The satisfied flow found after all was the boundary layer developed on a flat plate with a straight wing having laminar profile NACA 66_3018 erected on it. (See Fig.6). Related experiments were carried out in a closed type low speed wind tunnel with a test section of 0.8×0.6 m in area and 1.52m long. The testing Reynolds number was $1.2\sim 1.3\times 10^6$ per meter and the turbulence intensity below 0.5%. The flat plate having a length of 1 m with its leading edge elliptically modified to prevent flow sepration was supported by the two side–walls of the test section. The straight wing with a chord of 660 mm erected on the flat plate was extended to the ceiling of the test section. (See Fig.6). A metal tripping wire 2mm in diameter was glued on the flat plate near the leading–edge for promoting the transition and forcing the boundary layer fully turbulent around the straight wing. The laminar profile has the property of having a long range of constant static pressure along its surface, which will produce a nearly uniform distribution of static pressure along the stream line (i.e.$\partial C_p/\partial s=0$) by the side of the wing, while keeping the transverse pressure gradient finite ($\partial C_p/\partial n\neq 0$). In order to prevent the flow from inducing horseshoe–vortex within the boundary layer near wing root, the leading–edge of the wing was modified to a spike form extruding forward. (See Fig.6). This modified part is rotatable about a pivot at 2.5% chord after the original leading–edge. For different angle of attack, the spike–like nose part was turned accordingly to keep the oncoming flow passing tangentially along the surface near the sharp leading–edge without separation which can be verified by testing. To determine the existence of the domain where pressure gradient $\partial C_p/\partial s=0$ and $\partial C_p/\partial n\neq 0$, static pressure distribution on the flat plate near wing–root was measured by using static pressure probes. The existence of $\partial C_p/\partial s=0$ was verified by the measured C_p vs. x curves as shown in Fig.7 and the values of $\partial C_p/\partial n$ were determined from the C_p vs. z curves (see Fig.8) for various measuring stations . The selected measuring stations located on a line L normal to the wing surface were situated at $x=210$mm behind the leading–edge. The measuring of turbulence quantities and data processing were proceeded in the same way as described in the case of $\partial C_p/\partial s\neq 0$ and $\partial C_p/\partial n=0$ case. After the $\overline{u'_s v'}$ and $\partial u_s/\partial y$ along the streamlines had been measured, the relations between K and $\partial C_p/\partial n$ for the inner layer as well as C and $\partial C_p/\partial n$ for the outer layer were determined as shown in Fig.9. These relations show the tendency that K and C decrease somewhat as the transverse pressure gradient increases. In order to verify the accuracy of the experiments, and to verify the measuring accuracy, measurements were made on a pure flat plate, and gave the relation: $u^+=5.51\log y^+ + 4.45$ which conforms with the general expression of the law of the wall: $u^+=5.62\log y^+ + 4.9$[3] pretty well. (See Fig.10), if the roughness of the flat plate and the turbulence of the wind tunnel are taken into account. Based on these experimental results,

the following empirical formulas were deduced:

$$\Delta K = K - K_{eq} = -0.45\delta^* \left(\frac{\partial C_p}{\partial n}\right) \tag{3}$$

$$\Delta C = C - C_{eq} = -0.092\delta^* \left(\frac{\partial C_p}{\partial n}\right) \tag{4}$$

where K_{eq} and C_{eq} are the K and C under the condition of equilibrium with $\partial C_p / \partial n = 0$, δ^* is the displacement thickness. The tendency of decreasing C with the increase of $\partial C_p / \partial n$ is in correspondence with the results of the NLR in Holland[7], which displays the C to decrease with the increase of the flow deflection angle β_w at the wall.

Additional equations needed for algebraic turbulence model to have memory and to take account of the effect of pressure gradient on K and C

As mentioned earlier, it can be assumed that the effect of the pressure gradient on algebraic model lies on varying the parameters K and C, and the historical effect of turbulence, ie. the nonequilibrium, rests on derivatives $\partial K / \partial S$ and $\partial C / \partial s$. Therefore, on purpose of improving the computation as a whole, the following two ordinary differential equations were introduced:

$$\lambda\delta\frac{dK}{ds} - \Delta K = K_{eq} - K \tag{5}$$

$$\lambda\delta\frac{dC}{ds} - \Delta C = C_{eq} - C \tag{6}$$

where λ represents a lag length of the variation, tentatively taking $\lambda = 2$, K_{eq} and C_{eq} were to be determined by the pressure coefficient β according to the empirical formulas, equation (1) and (2). For example, the Reynolds shear stress can be expressed as $\tau_t = \rho l^2 (\partial u / \partial y) |\partial u / \partial y|$, where l is the mixing length which can be express as $l / \delta = C \tanh (Ky / C\delta)$ according to the Michel's model. Here the parameters K and C are no longer constant as commonly used, but should be determined by simultaneously solving the equations (5) and (6) with the boundary layer equations. How much actually the improvement could be got through using the proposed algebric turbulence model would be examined via the computation of the following test cases.

Ⅲ. Computational test cases

In order to validate the computational results by solving boundary layer equations along with the newly proposed algebraic turbulence model , five potentially useful test cases having measuring data were adopted for computation.

Case 1. A cylinder standing on a flat plate

This case concerns with the boundary layer developed in front of a cylinder standing on a flat wall in a wind tunnel. The experiment was described in R.Dechow and K.O.Felsh[8], TH. Karlsruhe, Germany. The cylinder diameter is 320mm with a streamlined afterbody to prevent separation. The sketch of the experimental setup is as shown in Fig.11 with the measuring stations indicated. Measurements were performed along the symmetry line (AS) at two stations and along an outer streamline (BC) at ten stations. Far upstream the boundary layer is two–dimensional. The non–circular cylinder induces a pressure distribution driving the boundary layer to three–dimensionality. Hot wire anemometer was used for velocity measurement and Preston tube for wall shear stress. In the computation[12], finite difference scheme was used for solving the two momentum equations with the continuity equation satisfied apart from joining the iteration. Because the continuity equation is linear, the iteration can be simplified without the continuity equation to join with. Using the Cartesian coordinates fixed on the flat plate as shown in Fig.11, the governing equations can be expressed as follows:

$$\begin{cases} \dfrac{\partial u}{\partial x} + \dfrac{\partial u}{\partial y} + \dfrac{\partial w}{\partial z} = 0 \\ u\dfrac{\partial u}{\partial x} + v\dfrac{\partial u}{\partial y} + w\dfrac{\partial u}{\partial z} = -\dfrac{1}{\delta}\dfrac{\partial p}{\rho x} + \dfrac{\partial}{\partial y}\left(\dfrac{\tau_{tx}}{\rho} + v\dfrac{\partial u}{\partial y}\right) \\ u\dfrac{\partial w}{\partial x} + v\dfrac{\partial w}{\partial y} + w\dfrac{\partial w}{\partial z} = -\dfrac{1}{\delta}\dfrac{\rho p}{\partial z} + \dfrac{\partial}{\partial y}\left(\dfrac{\tau_{tz}}{\rho} + v\dfrac{\partial w}{\partial y}\right) \\ \dfrac{\partial p}{\partial y} = 0 \end{cases} \tag{7}$$

where ρ is the density and p is the pressure ,the terms $-\frac{1}{\rho}\frac{\partial p}{\partial x}$ and $-\frac{1}{\rho}\frac{\partial p}{\partial z}$ can be determined by solving the potential equation of the flow outside the boundary layer, and the turbulent shear stresses $\tau_{tx} = -\overline{u'v'}$ and $\tau_{tz} = -\overline{w'v'}$. The boundary conditions are: $u = v = w = 0$ at $y = 0$ and $u = u_e, w = w_e$ at $y = \infty$.

The boundary layer equations were first transformed by a similarity transformation for the purpose of reducing the growing rate of the boundary layer and then discretized by using the box scheme which is an implicit scheme with second order precision as suggested by H. B. Keller[9]. All derivatives were approximated by two–point centered difference. Finally the discretized equations were solved by the Newton / Raphsen procedure. Calculation can be started by reading in initial profiles at formost station and to proceed downstream. The initial velocity profiles were gained from experiments at formost location in front of the cylinder and that in the symmetrical plane ($z = 0$) gained by solving the boundary layer equations for symmetrical plane. Several conventional turbulent stress models were employed to compare with the proposed model. Among these was the Michel's expression[10]: $l / \delta = C \tanh \left(\frac{K}{C}\frac{y}{\delta}\right)$ modified by multipling on righthand side the V. Driest's damping facter $[1 - \exp(-y / A)]$ with a the damping length A defined as $26(\tau_w / \rho)^{-\frac{1}{2}}\nu$.

Other algebraic turbulence models used in the computation were Cebeci–Simth and Mellor–Herring's. Their

expressions can be found in the literature[3]and needn't be recited here. In the computation, factor of anisotropism $T = \nu_{tnn} / \nu_{tss}$ as suggested by J. C. Rotta[25] was introduced to consider the anisotropic variation of the eddy viscosity ν_t. Here for three dimensional boundary layer ν_t can be expressed as:

$$\nu_t = l^2[(\frac{\partial u}{\partial y})^2 + (\frac{\partial w}{\partial y})^2 - (1-T)h^2]^{\frac{1}{2}} \qquad (8)$$

with $h = \frac{w}{u_r}\frac{\partial u}{\partial y} - \frac{u}{u_r}\frac{\partial w}{\partial y}$ and tentatively T=0.8.The convergence criterion for the iteration in computation was taken as: $|\delta s_w / s_w| < \varepsilon'$and $|\delta t_w / t_w| < \varepsilon'$ where $s_w = (\frac{\partial u}{\partial \eta})_{\eta=0}$ and $t_w = (\frac{\partial w}{\partial \eta})_{\eta=0}$ with $\varepsilon' = 10^{-2}$.

Computational and experimental data are presented in form of curves which include the distribution of velocity components in streamline coordinate (Fig.12), wall frictional coefficient C_{fw} (Fig.13), Reynolds stresses (Fig.15) and the thickness δ^* along a definite streamline BC (Fig.14). These curves illustrate that, in general, the Cebeci–Smith or the Michel's model seems fitting better, although the Mellor–Herring's model could give satisfiable results for δ^* and C_{fw}, but neither of them could predict the Reynolds stresses with sufficient accuracy. The deviation existing between the computation and experiment is greater as the adverse pressure gradient becomes stronger when moving towards the cylinder. However the results gained by using the proposed new model will improve at any rate the accuracy of prediction, especially for the distribution of Reynolds stresses. In these mentioned figures, curves of turbulent stresses with or without considering the effect of $\partial C_p / \partial n$ are presented , therefore how much the revised quantities can be contributed by the $\partial C_p / \partial n$ term can be discerned. However the accuracy concerning the prediction of the turbulent stress in z–direction τ_{tz} is still unsatisfactory, although the improvement is obviousely achieved by using the proposed new turbulence model.

Case 2. A tapered cylinder standing on a flat plate

Instead of employing circular cylinder as described in Case 1, here a tapered cylinder with a tear–drop profile was erected on the flat plate. Relevant experiments were conducted by F.J. Pierse et al. of VPI and state university[13], virginia, USA, They provided data appropriate for validating the three dimensional turbulent boundary layer code. There are measured boundary layer edge condition which can eliminate the need of assuming a freestream potential flow for computation. The experiments were conducted in an open circuit low speed wind tunnel having a cross–section area of 0.61 × 0.91m. The freestream turbulence intensity was about 0.5%. The wall shear stress was measured by Preston tube and the Reynolds stresses by hot wire / film probes. The initial condition plane was located 24 inches upstream of the body leading edge, where the profile of mean velocity and the six Reynolds stresses had been measured at several stations. The measuring stations are as shown in Fig.16, from which only the stations 1, 2 and 3 located at places with their x– and y–coordinates (-7,0), (–5,0) and (–7,–6) respectively were selected for computation to compare with the measurement. The same computational method as described in Case 1 was used in this case, except the pressure distribution data were adopted from experiments instead of the potential solution. From the curves drawn in Fig.17 to Fig.21, the effectiveness of using the proposed new model on improving the computational accuracy can be discerned. In order to validate the effect of using new model, calculation was proceeded under three conditions, i.e. 1) for constant K and C, 2) for K and C varying according to the expression (1) and (2) with $\partial C_p / \partial n = 0$, $\partial C_p / \partial s \neq 0$ and 3) for K and C varying with $\partial C_p / \partial n \neq 0$ and $\partial C_p / \partial s \neq 0$ for station 3 standing apart from the symmtrical plane. Computational results show that for all examined turbulence models, the bulk quantities such as δ^*, θ, u corresponds relatively well to the experiments exept in the inner layer and the measuring station near to the separation line. However the transverse velocity w does not agree satisfactory to the measuring data. The deviation is clear for the stations standing apart from the symmetric plane. The new proposed model can also increase the predictional accuracy of the wall friction. For example, the measured C_{fw} equals 2.35×10^{-3} at station 2, while the computational values corresponds to conditions 1), 2), and 3) are 2.5×10^{-3}, $2.4 \times 10^{-3}$and 2.25×10^{-3} respectively. That means the computational values will decrease to approach the experimental value when the effect of the pressure gradient is considered, even though it may under–estimate somewhat in condition 3). As has been mentioned, there are apparent deviation between the predicted and the experimental data of the Reynolds stresses for most of the models used. Their predicted values are always over–estimated. But by using the proposed turbulence model the estimated value will reduced to approach the experimental data closer than other models as shown in Fig.20 and Fig.21. It is evident that the tendency of improvement is correct when the pressure gradient and historical memory effects are taken into account. By the way, it deserves to mention that the experimental tendency of monotonic increase of the transverse stress τ_{tz} till very adjacent to the wall (Fig.21) seems unusual comparing with other experimental examples, if the local pressure gradient is not severely strong.

Case 3. A straight wing having a profile of circular leading–edge and rectangular middle part tapered to a sharp trailing–edge standing on a flat plate

In this case, the behavior of the pressure induced

three dimensional boundary layer developed on the flat plate was investigated experimentally by L.F.East[14] in England early in 1971, who had measured the general behavior of the boundary layer besides the turbulent stresses. The measurement of the turbulent stresses under same condition was implemented by the author and his students[15]. By measurement, we used hot wire / film probes, Preston tube and wall hot film. Details can be found in Reference[1]. The computational method used in this case was same as described in case 1, except the initial velocity distribution in front of the obstacle and the pressure distribution outside the boundary layer were taken from the experiments. Curves illustrating the variation of the Renolds stress along the direction of local stream line in plane parallel to the plate for different stations together with the experimental data are shown in Fig.22. Although the agreement between the computation and experiment is not so well as expected, but considering the pressure gradient and the historical evolution of the turbulence will effectively increase the accuracy of prediction, i.e. the improvement achieved by using the proposed new model is rather evident.

Case 4. A case of simulation of the flow past an infinite 35 ° swept wing

The experiment simulating a flow past an infinite 35 ° swept wing was performed at NLR, Holland in a 3 × 2m low speed wind tunnel conducted by B. Van den Berg[16] and A. Elsenaar[17]. In experiment, the initial two–dimensional boundary layer on the test plate was subjected to adverse pressure gradient, which led to three–dimensional separation near the trailing edge of the plate. Velocity profiles, skin friction and Reynolds stresses were measured at stations shown in Fig.23. The boundary layer was maitained very nearly quasi–two–dimensional with the help of guide vanes on either side of the region investigated. The direction and the magnitude of the velocity at the boundary layer edge were measured with a cylindrical yaw tube and a Pitot static tube respectively. The velocity measurements inside the boundary layer were carried out with a rotatable hot wire probe. The magnitude of the skin friction and its direction was determined by wall Pitots of the Stanten type. Since there are regions with high pressure gradient and flow separation in downstream, the Baldwin–Lomax turbulence model claimed suitable for separated flow was employed in addition. The Baldwin–Lomax model is basically a two layer model having a same expression for eddy viscosity in inner layer as that of Cebici–Smith's, but in the outer layer, function F_{wake} is introduced instead of $q_e \delta^* = \int_0^\infty (q_e - q)\,dy$, here $q = (u^2 + w^2)$. Details can be found in the literiture[18]. Also the k–ε two equation model in type of Chien's low Reynolds number form[19][20] is employed for computation to compare with the results obtained by using algebraic models. In Chien's model, the dissipation rate ε is replaced by $\varepsilon = \tilde{\varepsilon} + D$ with $D = 2\gamma k / y^2$ and the eddy viscosity $\gamma_t = C_\mu f_\mu R_t$ with $R_t = k^2 / (\gamma\tilde{\varepsilon})$, $R_y \sqrt{ky} / \nu, C_\mu = 0.09$, and $f_\mu = 1 - exp(-0.0115y^+)$. The k and ε equations which can be found in the literature[19] are omitted here. The boundary conditions used are: $u = v = v$, $\tilde{\varepsilon} = 0$ and $k = 0$ for $y = 0$; and $u = u_e(x), w = w_e(x), u_e \partial k / \partial x = -\tilde{\varepsilon}$ and $u_e \partial\tilde{\varepsilon}^2 / \partial x = -c_2 f_2 \tilde{\varepsilon}^2 / k$ with $c_2 = 1.8$ for $y = \infty$. For this quasi–two –dimensional flow it is appropriate to introduce a stream function. Hence the continuity equation is satisfied and only two momentum equations along with the closure k–ε equations need to be solved. Using a similar numerical method as described in case 1, the process is to solve iteratively first the momentum equations then the k and ε equations till the criterion of convergence $\left|(\partial u / \partial\eta)^{\eta}_{\eta=0} - (\partial u / \partial\eta)^{\eta-1}_{\eta=0}\right| < 0.001$ is satisfied. Since the governing equations are of parabolic type, the discretized finite difference equations can be solved[21] starting from the initial position $x_m = 0.426$ m which conincides with the first measuring position and marching downwards. The initial velocity and k profiles were obtained from experiments, while the initial ε profile obtained primarily by estimation.

In Fig 24, the profile of the velocity component tangential and normal to the direction of flow outside the boundary layer are drawn for various turbulence models. It can be seen that as x_m increases approaching to the separation line, the predictional results of all models deviate not only from each other but also from the measurement.

The results of distribution of fricitonal coefficient along x_m–direction are illustrated in Fig 25. It can be seen that using the present turbulence model will provide a better result than others. The computational value of C_f deviate from the measured data gradually as the separation line (nearly at $x_m = 1.3m$) is approached, even the computation can continue to pass over the separation point. In Fig.26, curves experessing the distribution of Reynolds stresses (i.e. correlation $\overline{u'v'}$ and $\overline{w'v'}$) in boundary layer at position $x_m = 0.995$m and at position near separation $x_m = 1.190m$ are drawn to compare the predicitonal results with the measurement. Despite of the discernible deviation existing between the measured and computational values, it is clear that the proposed turbulence model seems superior to the other models in prediction.

Case 5. boundary layer flow in the symmetrical plane of a 6:1 prolate spheroid at incidence

The experiments of this test case were carried out by H. U. Meier et al[22]. at Goettingen with the prolate spheroid located in the 3 × 3m test section of a low speed wind tunnel. The spheroid had major and minor

axis of 2.4m and 0.4m respectively. The testing Reynolds number was 7.7×10^6 and the turbulence intensity of the order of 0.2%. Wall shear stresses were measured by hot film gauges flush mounted with equal spacing along the model. In the computation, the transition is assumed in the middle of the experimentally observed transition region which extends physically the spheroid over approximately 15% of its length. The coordinates used for computation is of elliptic system with the basic vectors x. n. φ directing to the wall meridian, the normal and the peripherally extended angle respectively with the origin located at the front stagnation point. After introducing the two-component vector potential ψ and Φ, so that $u=\partial\psi/\partial y$, $w=\partial\Phi/\partial y$ and $v=-(\partial\psi/\partial x+\partial\Phi/\partial z)$, the continuity equation is satisfied. By solving the discretized momentum equations[24], Keller's method was used again with the velocity outside the boundary layer deduced from the potential solution for boundary condition. Since only limited experimental data are avaible by us, here merely the comparison of the C_f distribution is presented in Fig 27. The apparent deviation between the predicted and experimental data near the end of the body at leeward plane can be attributed to the difference of pressure distributionof potential flow used in computation and in real case. Through comparison, it can be seen that using the proposed new turbulence model can improve the predictional accuracy too in this case.

Ⅳ. Conclusion

In order to increase the predictional accuracy, an algebraic turbulence model based on experiments is proposed to take account of the effect of pressure gradient and turbulence nonequilibrium by introducing two additional first order ordinary differentail equations. Five test cases including the boundary layers developed on flat plates with obstacles standing on them, the boundary layer field simulating the flow around a back-swept wing and the flow past a prolate spheroid with slenderness ratio 1 / 6 in symmtrical plane were selected to validate the predicitonal accuracy in comparison with the exprimental data. The comparion reveals that using the proposed algebraic turbulence model with memory will gain an apparent improvement in prediction of the behavior of three dimensional turbulent boundary layers, especially for the distribution of turbulent stresses.

Acknowledgment

The auther is grateful to his former students Dr. L.Wang, Dr. W. H. Kuo, Dr. candidate L. Yuan, Mr. B. Xue and Mr. X. Y. Wang for the work they did together with me, which are directly or indirectly helpful to the completion of the present work, during their stay in BUAA.

References

[1] Hsing, T.D. Teng, H. Y., AIAA Paper 84-1529, 1984.
[2] Wang, L., Hsing. T. D., Proc. of the 3rd Conf. on Fluid Mech in China, 1985.
[3] Cebeci, T., Smith, A. M. O., Analysis of Turb. Boundary Layers, Academic Press. 1974.
[4] Townsend, A. A., Journal of Fluid Mech. 11, 97, 1961.
[5] Mellor, G. L., Gibson, D. M., Journal of Fluid Mech. 24, 225, 1966.
[6] Glowucki, W. J., AIAA Paper 78-202, 1978.
[7] Johnston, L. J., Aeronautical Journal, 115-131, April, 1989.
[8] Dechow, R. et al., Mitteilungen, TH. Karlsruhe, Heft 21.
[9] Keller, H.B., A new difference scheme for parabolic problems. In: Numerical Solution of Partial Differential Equations Ⅱ, SYNSPADE, Academic, N.Y.
[10] Michel, R., Proc. Comp. Turb. Boundary Layers, AFOR-TEP-Stanford Conference, vol.1, 195-212A.
[11] Hsing, T. D., Xue, B., Proc. of the 1st International Conference on Experimental Fluid Mechanics, China, 1991.
[12] Hsing, T. D., Guo, W. H., Wang, L., Proc. of the 3rd International Symposium on Refined Flow Modelling and Trubulence Measurements. 43-51, Tokyo, 1988.
[13] Pierce, F. J. , et al.,Journal of Fluid Engineering, Dec. 1988; and Rept. VPI-E-84-23, June 1984.
[14] East, L. F., et al., R. & M. No. 3653, Royal Aeronautical Society, 1971.
[15] Hsing, T. D., et al., ACTA AERONAUTICA ET ASTRONAUTICA SINICA, Vol. 5, 4.1984.
[16] Van den Berg, B., et al., NLR TR 72092U, Holland, 1972.
[17] Elsenaar, A., NLR TR 74095U, Holland, 1974.
[18] Baldwin, B. S., Lomax, H., AIAA Paper 78-257, Jan. 1978.
[19] Patel, V. C., Rodi, W., Scheuerer, G., AIAA J. vol. 23, No.9, 1308-1379, Sept 1985.
[20] Chien, K. Y., AIAA J. Vol.20, No.1, 33-38, Jan 1982.
[21] Yuan, L., Hsing, T. D., BUAA Paper BH-B3685, Proc. of the 4th Symposium on Turbulence and Flow Stability in China, 1991.
[22] Meier, H. U., Kreplin, H. P., Z. F. W. 4, H. 2, 65-71, 1980.
[23] Kuo, W. H., Hsing, T. D., BUAA Paper BH-B2391, presented to the 3rd Symposium on Turbulence and Flow Stability in China, 1987.
[24] Wang, X. Y., BUAA Master thesis, 1988.
[25] Schneider. G. R., Deutsche Luft- und Raum faht FB77 -73, Goettingen, 1977.

Figures

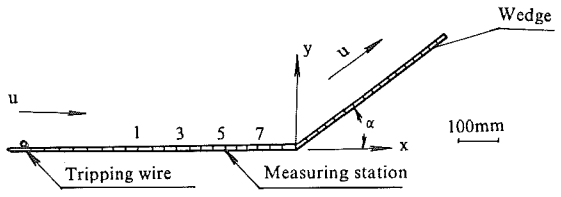

Fig.1 Wedge shaped experimental setup for studying the effect of $\frac{\partial C_p}{\partial s}$ on eddy viscosity

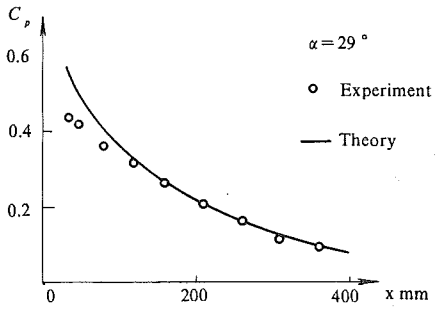

Fig.2 Static pressure coefficient distribution toward wedge surface at α=29 °

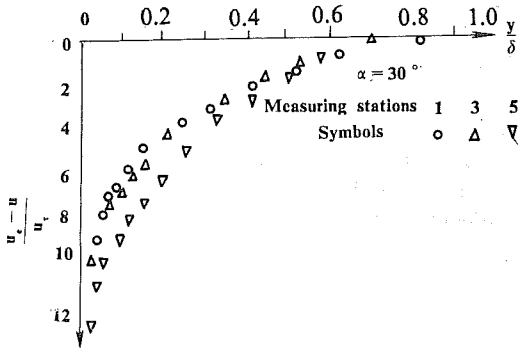

Fig.3 Velocity-defect profiles at various measuring stations for wedge deflection α=30 °

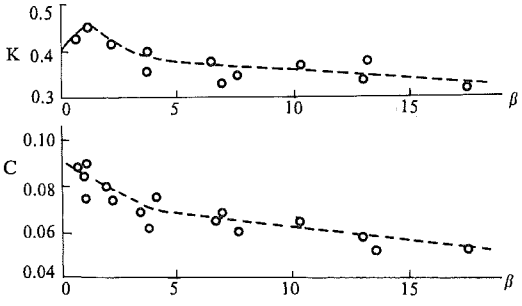

Fig.4 Measured variation of parameters K and C with the transvevse pressure gradient

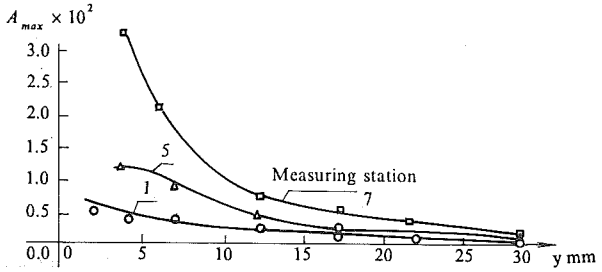

Fig.5 Distribution of the peak spectrum density along y-axis normal to the surface at various measuring stations

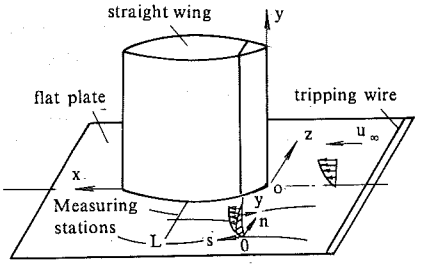

Fig.6 Sketch of model instatllation and measuring stations in region $\frac{\partial C_p}{\partial s}=0, \frac{\partial C_p}{\partial n}\neq 0$ for studying the effect of $\frac{\partial C_p}{\partial n}$ on eddy viscosity

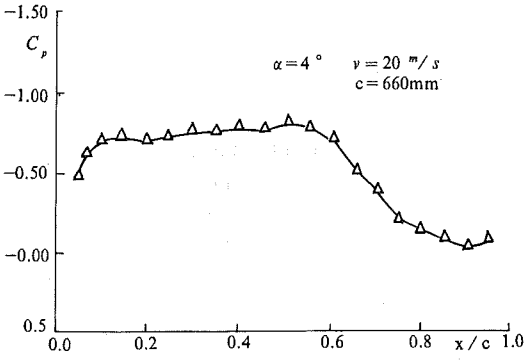

Fig.7 Pressure distribution showing $\frac{\partial C_p}{\partial s}=0$ at measuring region

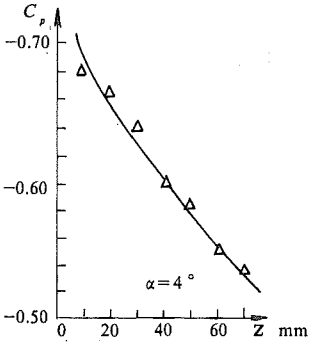

Fig.8 Pressure distribution showing $\frac{\partial C_p}{\partial n}\neq 0$ at measuring region for incidence α=4 °

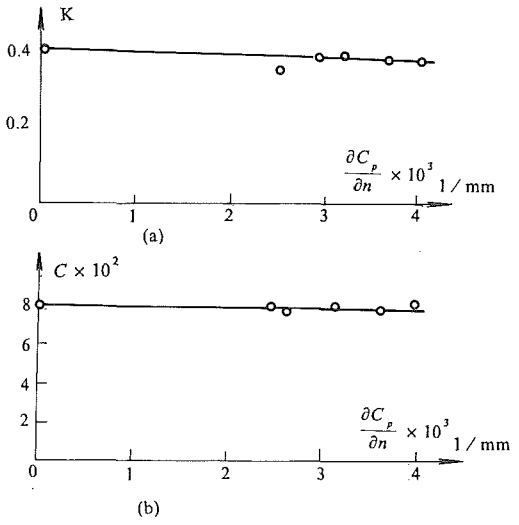

Fig.9 Curves of K and C versus $\frac{\partial C_p}{\partial n}$

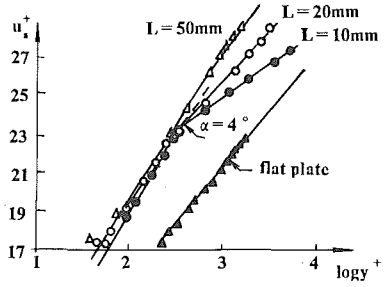

Fig.10 Velocity distribution curves for flat plate and plate with wing at incidence $\alpha = 4°$ measuring at L = 10, 20 and 50 mm normal to the wing surface

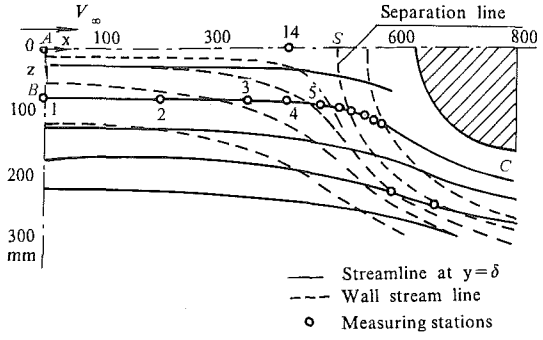

Fig.11 Streamline pattern around test setup of Case 1 and positions of measuring stations [8]

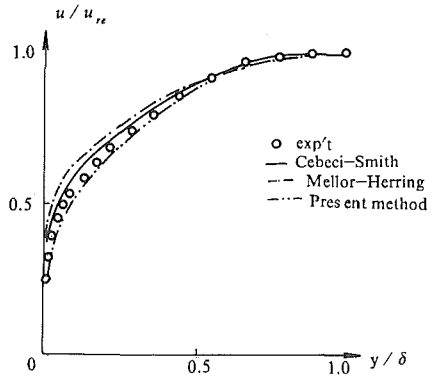

Fig.12 Computational velocity distribution curves in comparison with the measuring data at No.5 station

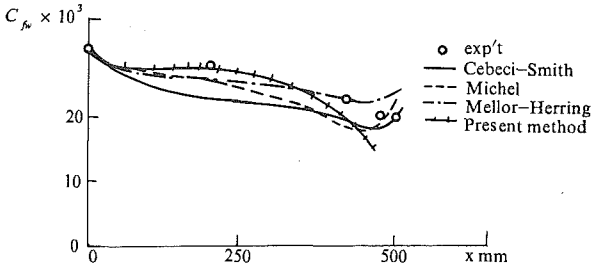

Fig.13 Coefficient of wall friction at stations along a streamline

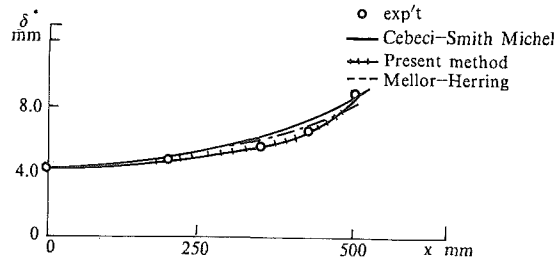

Fig.14 Displacement thickness distribution along a streamline

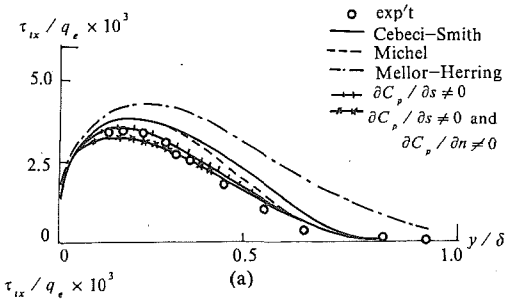

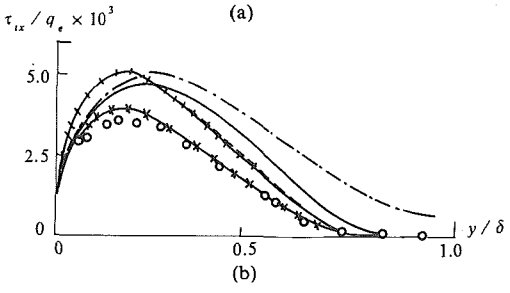

Fig.15 Distribution of turbulent stress ratio τ_{tx}/q_e vs.y/δ : (a) at station 4 and (b) at station 5

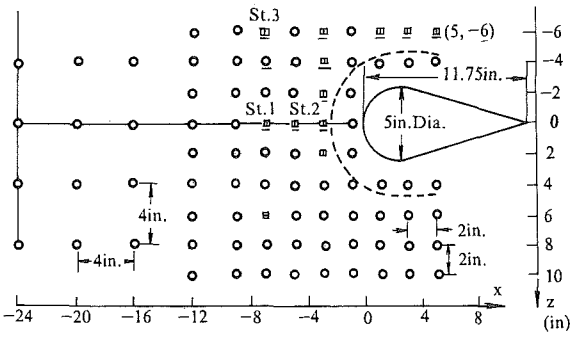

Fig.16 Test setup of Case 2 and the positions of measuring stations [13]

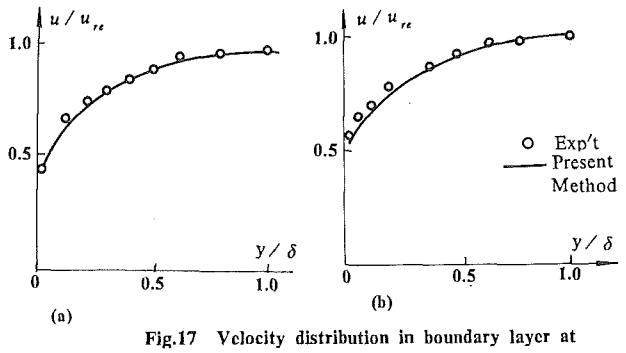

Fig.17 Velocity distribution in boundary layer at positions: (a) No.1 and (b) No.3 stations

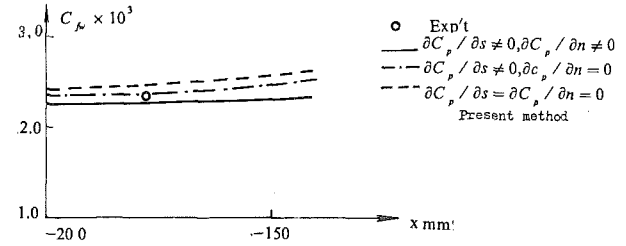

Fig.18 Coefficient of wall friction on positions along x direction with z = 6 in.

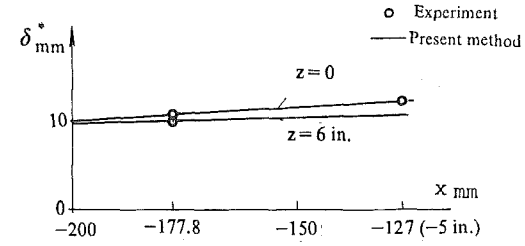

Fig.19 Displacement thickness distribution in boundary layer along x direction for z=0 and z=6 in. (152.4mm)

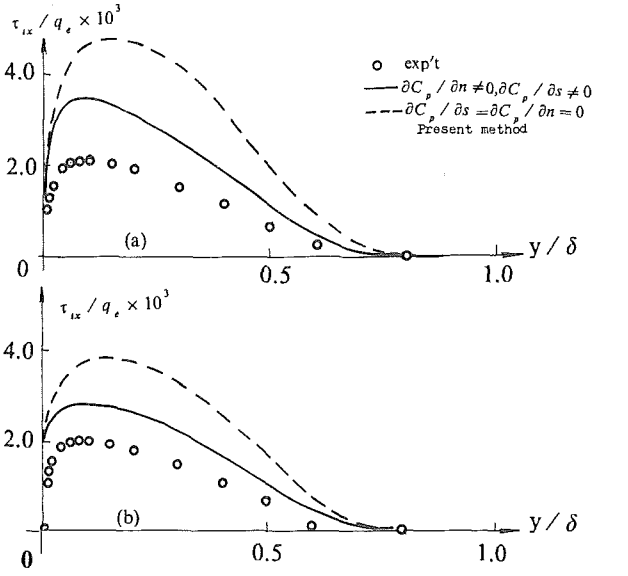

Fig.20 Distribution of turbulent stress ratio τ_{tx} / q_e vs. y / δ at: (a) station 1 and (b) station 2

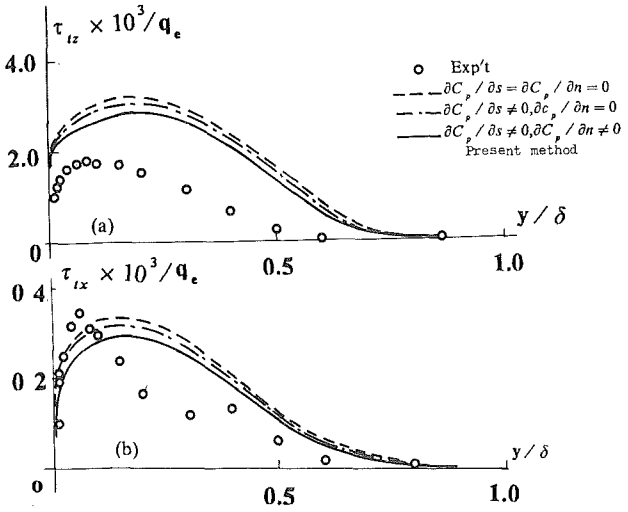

Fig.21 Distribution of turbulent stresses ratio: (a) τ_{tx} / q_e in x-direction and (b) τ_{tz} / q_e in z-direction vs. y / δ

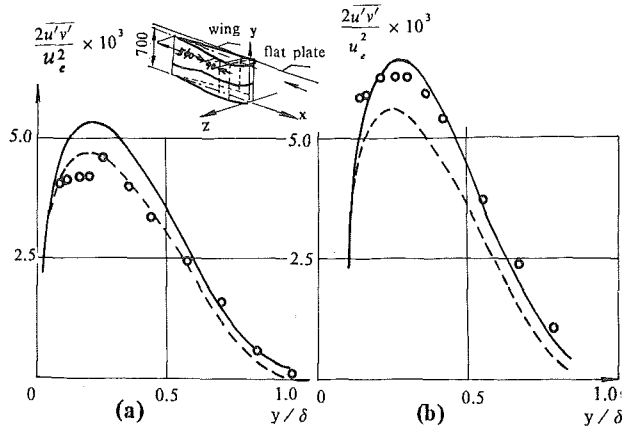

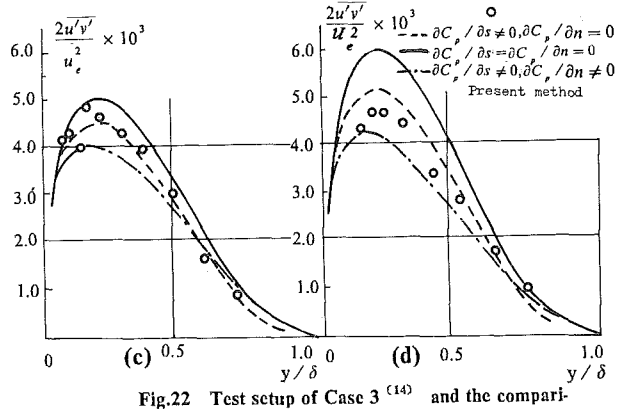

Fig.22 Test setup of Case 3 [14] and the comparison of computational turbulent stress distributation to experimental results measured at positions: (a) x=125, z=0, (b) x=105, z=0, (c)x=125, z=30 and (d) x=105, z=30

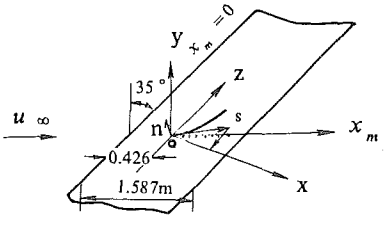

Fig.23 Plane form of the 35° swept infinite wing and the coordinate systems[16]

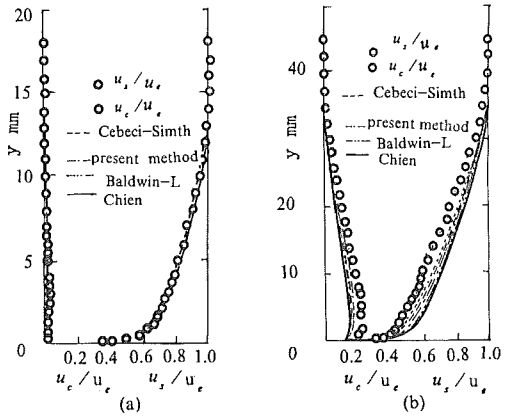

Fig.24 Comparison of the computational and experimental results for the streamwise and transverse velocity distribution within the boundary layer at positions: (a) $x_m = 0.62$m and (b) $x_m = 1.12$m

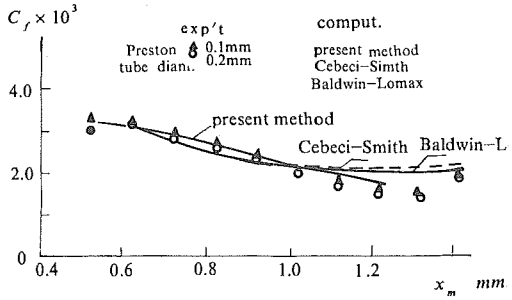

Fig.25 Distribution of the coefficient of wall friction along x_m–axis

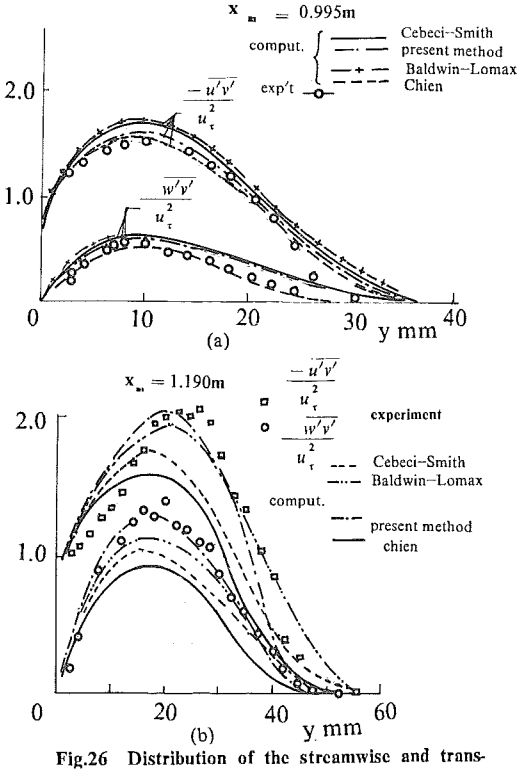

Fig.26 Distribution of the streamwise and transverse turbulent stresses along y–axis normal to the surface at positions: (a) $x_m = 0.995$m and (b) $x_m = 1.190$m

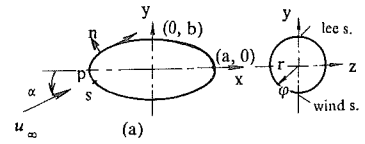

Fig.27 (a) Side and front view of the prolate spheroid in Case 5 [22] with slenderness ratio 1:6 and the coordinate systems

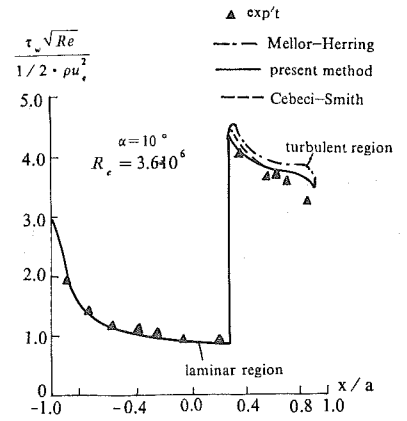

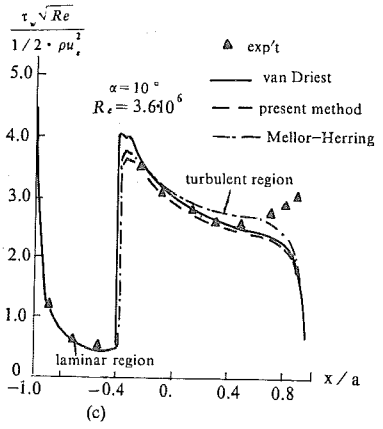

Fig.27 (b) and (c) Distribution of the coefficient of wall friction along x–axis on: (a) leeward and (b) windward side